On the Role of Coronal Shocks for Accelerating Solar Energetic Electrons

Nina Dresing, Athanasios Kouloumvakos, Rami Vainio, Alexis Rouillard

The Astrophysical Journal Letters, 925:L21 (7pp), 2022 February 1 https://doi.org/10.3847/2041-8213/ac4ca7

On the Role of Coronal Shocks for Accelerating Solar Energetic Electrons

Nina Dresing[1,2], Athanasios Kouloumvakos[3], Rami Vainio[4], and Alexis Rouillard[3]
[1] Department of Physics and Astronomy, Turku Collegium for Science, Medicine and Technology, University of Turku, Finland; nina.dresing@utu.fi
[2] Institut für Experimentelle und Angewandte Physik, Universität Kiel, D-24118, Kiel, Germany
[3] IRAP, Université Toulouse III—Paul Sabatier, CNRS, CNES, Toulouse, France
[4] Department of Physics and Astronomy, University of Turku, Finland
Received 2021 November 25; revised 2022 January 17; accepted 2022 January 17; published 2022 February 2

Abstract

We study the role of coronal mass ejection (CME) driven shocks in the acceleration of solar energetic electrons. Using observations by the two STEREO spacecraft, we correlate electron peak intensities of solar energetic particle events measured in situ with various parameters of the associated coronal shocks. These shock parameters were derived by combining 3D shock reconstructions with global modeling of the corona. This modeling technique provides also shock properties in the specific shock regions that are magnetically connected to the two STEREO spacecraft. We find significant correlations between the peak intensities and the Mach number of the shock with correlation coefficients of about 0.7, which are similar for electrons at ∼1 MeV and protons at >60 MeV. Lower-energy electrons with <100 keV show a smaller correlation coefficient of 0.47. The causal relationship between electron intensities and the shock properties is supported by the vanishing correlations when peak intensities at STEREO A are related with the Alfvénic Mach number at the magnetic footpoint of STEREO B and vice versa, which yields correlation coefficients of 0.03 and −0.13 for ∼1 MeV and <100 keV electron peak intensities, respectively. We conclude that the high-energy electrons are accelerated mainly by the shock, while the low-energy electrons are likely produced by a mixture of flare and shock-related acceleration processes.

Unified Astronomy Thesaurus concepts: Active sun (18); Solar coronal mass ejection shocks (1997); Interplanetary particle acceleration (826); Solar flares (1496); Solar energetic particles (1491); Solar particle emission (1517)

1. Introduction

The classic two-type picture of solar energetic particle (SEP) events (Reames 1999, 2021a) assumed two distinct acceleration processes for impulsive and gradual events. Impulsive, electron-rich events, which are characterized by their special elemental composition (e.g., rich in ^{3}He; Cane et al. 1986; Reames 2021b), their impulsive time history, and small angular extent, are attributed to particle acceleration from magnetic reconnection in solar jets and flares. Gradual, proton-rich events are believed to be generated by coronal mass ejection (CME) driven shocks that accelerate and inject SEPs over longer times and that produce events with larger angular extents corresponding to the larger acceleration region. It is accepted that energetic electrons, which cause the hard X-Ray (HXR) flare emission, when precipitating back into the solar chromosphere, are accelerated within magnetic reconnections in closed field regions (Mann 2015) to tens of keV. They can also be injected into open magnetic field lines connecting the sites of acceleration in the corona with the heliosphere. These propagating electron beams cause type III radio bursts and can eventually be observed in situ. The connection between the flare and these in situ electrons is supported by strong correlations between the spectral indices of the HXR flare and the corresponding in situ electron event (Krucker et al. 2007; Dresing et al. 2021; Wang et al. 2021).

The role of shocks in accelerating solar energetic electrons, especially to energies of more than ∼100 keV, is, however, still unclear. The close temporal relationship of flares and CMEs, and the usual presence of flares during CME-associated events make it difficult to separate potential flare-related and shock-related components in particle acceleration (e.g., Kouloumvakos et al. 2015). Interplanetary shocks crossing spacecraft located near 1 au have been shown to be nearly inefficient in accelerating electrons to energies of several tens to hundreds of keV (Tsurutani & Lin 1985; Dresing et al. 2016; Yang et al. 2019). However, exceptional electron-shock spikes of hundreds of keV or even MeV energies were found in Ulysses (Simnett 2003) and Voyager (Sarris & Krimigis 1985) observations at distances of 1.35 and 1.9 au, respectively. Furthermore, Masters et al. (2013) reported that Saturn's high-Mach-number bow shock accelerates electrons up to MeV energies. It seems therefore possible that specific conditions can be favorable for efficient electron acceleration at shocks (e.g., Mann et al. 2018), and these might also be met close to the Sun.

The classic dichotomy of SEP events between impulsive and gradual is, however, not present in all events. Previous statistical studies highlight the possibility that both flare- or shock-related acceleration processes can contribute to the acceleration of energetic electrons and protons (e.g., Kouloumvakos et al. 2015; Trottet et al. 2015; Papaioannou et al. 2016). Strong correlations between relativistic electron and deka-MeV proton flux increases (Posner 2007) suggest a common, possibly shock-related source of the two species. The velocity dispersion analyses of the 2011 March 21 SEP event, measured along magnetic field lines rooted at an estimated 90° in heliolongitude away from the flare site, gave similar particle release times for electrons and protons, suggesting a common shock origin (see Figure 11 of Rouillard et al. 2012). Also other features of solar energetic electron (SEE) events led authors to attribute them to shocks. These were, for example, gradual rising phases in well-connected events, or the frequently observed onset delays, suggesting a continuous or

delayed electron injection at the Sun with respect to the flare, respectively (Haggerty & Roelof 2002, 2009; Kouloumvakos et al. 2015). However, also processes related to particle transport, the electron injection at the Sun, and instrumental effects can be involved in producing such features (e.g., Dresing et al. 2020, 2021) and therefore prevent a clear shock association to SEE events so far. Long-lasting electron anisotropies marking temporally extended electron injections close to the Sun might be a strong indication for electron-shock acceleration as suggested also by Kahler et al. (2007). However, even such features can be produced by alternative processes, e.g., ongoing acceleration or trapping in post-flare loops (e.g., Klein et al. 2005) or CME−CME interaction regions (e.g., Gopalswamy et al. 2004; Dresing et al. 2018), where continuous leakage from the trap would cause the ongoing electron injection.

Dresing et al. (2020) analyzed a large sample of near-relativistic SEE events observed with the two STEREO spacecraft and found evidence for the presence of at least two types of electron events. They found long rise-time events associated with hard spectral indices as well as with the presence of higher-energy (>0.7 MeV) electrons, which could not be explained by a purely flare-related scenario. They, therefore, suggested an additional acceleration mechanism to be involved for these events that provides a prolonged particle injection.

The clear shock association of large energetic proton events was underlined by the strong correlation between 20 and 100 MeV proton peak intensities and shock parameters at magnetically well-connected regions to the observing spacecraft that Kouloumvakos et al. (2019) determined from 3D reconstructions and modeling of the observed pressure fronts. The strongest correlations were found with the strength of the shock as quantified by its Mach number.

In this work we make use of the two latter studies and combine their results. Namely we compare shock parameters for 33 large SEP events modeled by Kouloumvakos et al. (2019) with key observations of SEE events provided by Dresing et al. (2020) to determine the potential role of shocks for electron acceleration.

2. Data Analysis

2.1. Data Selection

Our study is based on the 33 coronal pressure waves modeled in 3D by Kouloumvakos et al. (2019) that occurred between 2011 and 2017. The modeled events were associated with energetic protons clearly detected in at least two locations in the heliosphere, at energies greater than 50 MeV. We compare this data set with the large sample[5] (781 events) of near-relativistic (55–85 keV) SEE events observed with the two STEREO spacecraft (Dresing et al. 2020). The two lists were synchronized based on temporal coincidence of the events, and false correlations, e.g., due to mixing of events observed closely in time, were excluded through manual inspection.

Table 1 presents the particle peak intensities for each of the 33 SEP events. Peak intensities of the near-relativistic electrons measured by the Solar Electron and Proton Telescope (SEPT; Müller-Mellin et al. 2007) are provided by Dresing et al. (2020). To complement these with relativistic electron measurements, we also determined the peak intensities of 0–7–1.4 MeV electrons provided by the STEREO High Energy Telescope (HET; von Rosenvinge et al. 2008). For comparison, Table 1 also includes the 60–100 MeV proton peak intensities that were used by Kouloumvakos et al. (2019). The bottom row of the table shows the number of events observed by each of the two STEREO spacecraft in the different channels, showing that the number of associated proton events (in total 54 events) is always higher than the corresponding electron events, which sum up to 50 (47) events at ∼1 MeV (<100 keV). There are various reasons for missing events. In most cases, no corresponding event could be identified. However, a few SEPT electron peak intensities were corrupted by ion contamination (IC), and some events were likely masked by a high pre-event background (High BG). In some other cases, no unambiguous corresponding peak intensity could be determined because of the mixing of events.

In the following section we analyze the relation between electron peak intensities and various shock parameters determined by Kouloumvakos et al. (2019) at the point where field lines passing the observer connect with the shock surface (termed the "cob-point"). For each event, the 3D structure of the shock wave is triangulated from images taken by STEREO and the Solar and Heliospheric Observatory (SOHO; e.g., Rouillard et al. 2016), then a global 3D megnetohydrodynamic (MHD) coronal model (PSI/MAST model; Lionello et al. 2009; Riley et al. 2011) is used to obtain the 3D distribution of basic shock parameters such as Mach numbers, compression ratios, and shock geometry $\Theta_{\rm Bn}$, which is defined as the magnetic field obliquity with respect to the shock normal (Kouloumvakos et al. 2019). The global MHD model is also used to derive the time-varying position of the cob-point specifically for each spacecraft measuring SEPs. To investigate the link between the SEP peak intensity and the shock parameters, Kouloumvakos et al. (2019) used the maximum values of the Mach numbers and compression ratios, while, for the shock geometry, they used the Θ_{Bn} value at the time when the Alfvén Mach number is maximum (see further details in Section 3 of Kouloumvakos et al. 2019). In our analysis we use the same shock parameter values.

2.2. Relating Solar Energetic Electron Intensities to Shock Parameters

Figures 1 and 2 show the correlations between energetic particle peak intensities and shock parameters at the cob-point. Each column shows the correlations of 55–85 keV electrons (left), 0.7–1.4 MeV electrons (center), and 60–100 MeV protons (right). Each row shows from top to bottom the correlations with the Alfvénic Mach Number M_A, the shock speed $V_{\rm sh}$, and the shock speed at the leading edge of the CME $V_{\rm sh}$ (LE). Figure 2 shows correlations of the shock geometry $\Theta_{\rm Bn}$ (top) and the shock connection height (center). Both shock parameters have been determined at the time when the M_A is maximum. The bottom row of Figure 2 shows the shock density compression ratio X.

Following Kouloumvakos et al. (2019), we determine the Pearson correlation coefficients of the logarithms of the peak intensities with the shock parameters. The logarithm was also used for the Alfvénic Mach Numbers. The legend of each panel in Figure 1 provides the correlation coefficient (cc) together with a determination of its uncertainty using the Fisher r-to-z transformation providing a 90% confidence interval. The lower-most number of each legend provides the p-value of

[5] http://www2.physik.uni-kiel.de/stereo/downloads/sept_electron_events.pdf

Table 1
Events and Corresponding Peak Intensities (in $cm^{-2}\ sr^{-1}\ s^{-1}\ MeV^{-1}$) of 55–85 keV Electrons, 0.7–1.4 MeV Electrons, and 60–100 MeV Protons for Events Analyzed by Kouloumvakos et al. (2019)

	STA Peak Intensities			STB Peak Intensities		
Date	SEPT e	HET e	HET p	SEPT e	HET e	HET p
2011-02-15	…	…	…	1.64E+04	3.46E-01	1.20E-02
2011-03-07	8.32E+02	1.32E+00	…	2.36E+04	1.51E+00	3.10E-02
2011-03-21	2.70E+05	1.71E+01	1.15E+00	…	…	…
2011-08-04	6.58E+02	2.10E-01	…	3.43E+02	1.94E-01	5.00E-03
2011-09-06	2.39E+02	…	3.00E-03	…	1.52E-01	5.00E-03
2011-09-22	IC	5.06E-01	1.10E-02	3.66E+05	3.16E+01	5.15E-01
2011-10-04	1.19E+04	7.90E-01	6.00E-03	4.84E+04	1.13E+00	1.50E-02
2011-11-03	9.55E+04	4.69E+01	2.81E-01	4.25E+03	7.97E-01	1.30E-02
2012-01-23	3.08E+04	2.15E+00	1.00E-02	1.89E+04	1.59E+00	1.60E-02
2012-01-27	IC	9.11E+00	5.10E-02	…	…	…
2012-03-05	…	…	…	1.21E+05	1.02E+01	3.70E-02
2012-03-07	2.33E+03	3.19E+00	3.00E-02	3.04E+05	3.37E+02	3.04E+00
2012-03-24	6.17E+04	2.15E+01	2.46E-01	2.75E+03	1.11E+00	8.00E-03
2012-05-17	IC	3.61E-01	8.00E-03	9.43E+01	9.95E-02	3.00E-03
2012-07-23	4.76E+06	7.92E+04	1.35E+01	4.92E+04	6.86E-01	2.00E-02
2012-09-20	2.87E+05	5.31E+01	2.47E-01	3.86E+05	8.73E+00	1.10E-02
2012-09-28	3.16E+05	1.67E+01	1.20E-02	1.75E+04	2.06E+00	1.20E-02
2013-03-05	4.54E+05	4.28E+01	1.73E+00	9.59E+03	2.14E+00	1.90E-02
2013-05-22	1.96E+04	…	…	2.53E+03	0.38	…
2013-10-05	4.61E+04	7.17E+00	2.90E-02	IC	2.23E-01	3.00E-03
2013-10-11	9.55E+04	3.00E+01	6.17E-01	9.19E+03	6.02E+00	8.50E-02
2013-10-25	1.38E+02	…	…	1.83E+04	1.32E+00	3.50E-02
2013-10-28	8.83E+02	1.23E-01	3.00E-03	8.83E+02	1.14E+00	2.40E-02
2013-11-02	6.48E+04	7.27E+00	2.30E-01	1.15E+03	2.30E-01	8.00E-03
2013-11-07	7.84E+04	4.81E+01	2.72E-01	1.06E+05	4.63E+00	1.14E-01
2013-12-28	IC	High BG	1.10E-02	High BG	High BG	1.50E-02
2014-01-06	2.35E+03	…	6.00E-03	2.21E+02	1.02E-01	6.00E-03
2014-01-07	…	DG	9.00E-03	3.55E+03	8.94E-01	8.00E-03
2014-02-25	5.49E+04	1.72E+01	9.30E-02	9.83E+04	3.76E+01	3.83E-01
2014-03-05	…	…	2.90E-02	…	…	7.60E-02
2014-09-01	DG	DG	DG	8.35E+05	1.91E+03	1.89E+01
2014-09-10	DG	DG	DG	1.63E+03	1.12E+00	8.00E-03
2017-09-10	4.53E+05	2.94E+01	4.50E-02	…	…	…
Total number	21	22	25	26	28	29

Note. DG: data gap; IC: ion contamination; High BG: high pre-event background.

the statistics. All correlation parameters are summarized in Table 2, which also includes the correlations with the fast magnetosonic Mach number $M_{\rm fm}$.

To allow for a qualitative comparison of the correlations of the different particle energies and species, we reduced the near-relativistic and the proton event sample to those events that were observed in the relativistic electron channel. Because the lower-energy electrons show fewer events in correspondence to the analyzed sample, the statistics are slightly worse. The number of associated proton events is the largest among the three analyzed groups, so that the sample used for the correlation was reduced.

Figure 1 and Table 2 show that the strongest correlations ($cc = 0.72$) are found for protons and the Alfvénic Mach number, followed by the fast magnetosonic Mach Number of $cc = 0.65$. While the correlation coefficients of high-energy electrons and protons are similar within the limits of uncertainties, the correlations of shock parameters with near-relativistic electron intensities are always weaker. However, in case of the magnetosonic and Alfvénic Mach Numbers and the shock speed, the correlation with the low-energy electrons gets stronger, when only considering events with peak intensities above $\sim 10^4\ cm^{-2}\ sr^{-1}\ s^{-1}\ MeV^{-1}$ (see Figure 1, left column). The correlations with the shock speed at the magnetic footpoints of the spacecraft (Figure 1, center row) are clearly stronger than the correlations with global value of the shock speed at the leading edge of the CME (Figure 1, bottom row).

No correlation is found between the SEP peak intensities and the shock obliquity $\Theta_{\rm Bn}$ (Figure 2, top) and also no differing trend between electrons and protons can be identified; both species show a tendency of the highest peak intensities of the sample to occur quasi-parallel to oblique shocks ($0 < \Theta_{\rm Bn} < 40$). The center and bottom rows of Figure 2 show that the correlations with the shock connection height and with the density compression ratio are weak, with even smaller numbers for the 55–85 keV electrons.

The bottom rows of Table 2 show that the correlations of protons with electron peak intensities are stronger than those with the shock parameters. While for the near-relativistic electrons the correlations weaken with increasing proton energy, it is the other way around for the relativistic electrons.

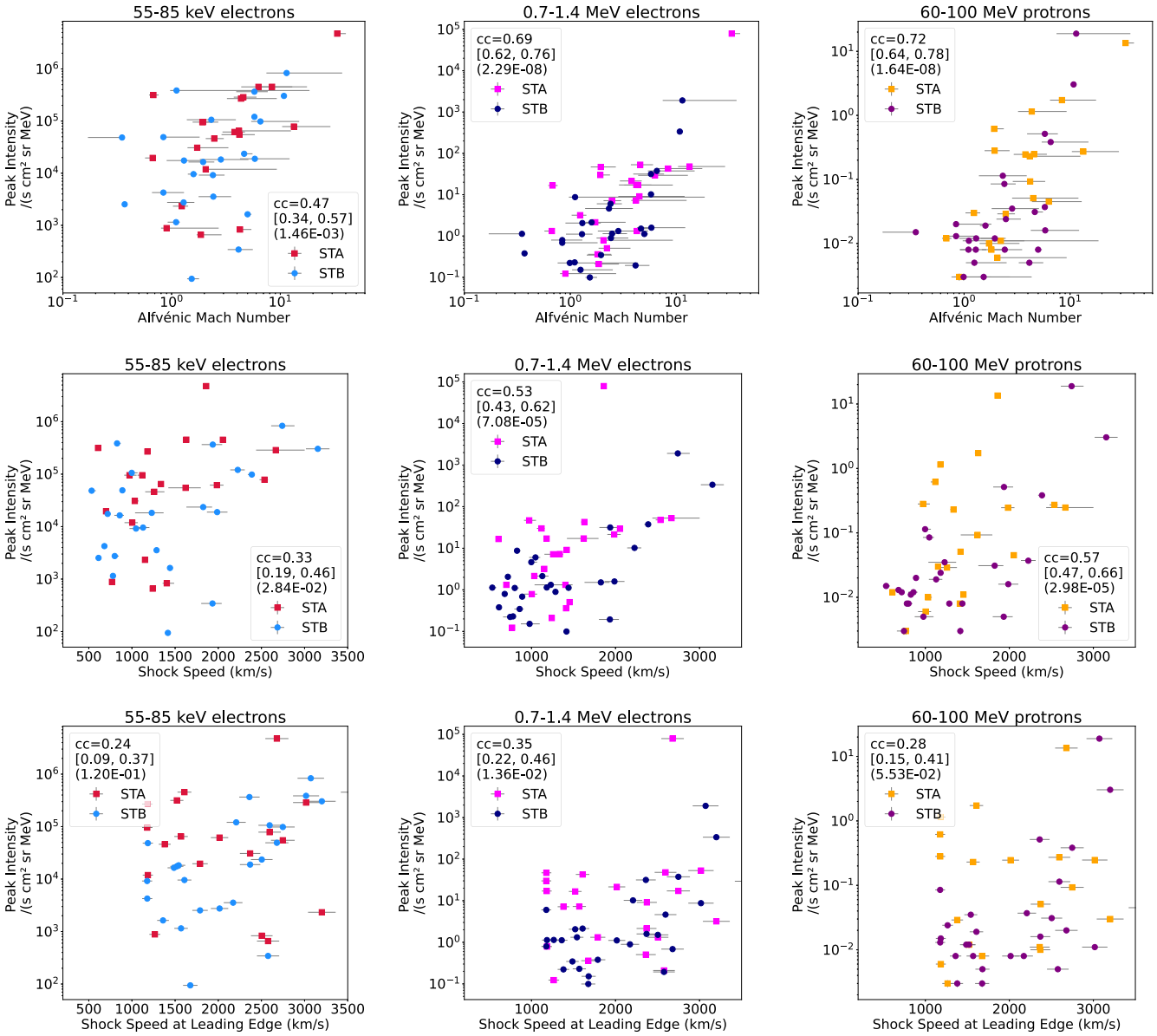

Figure 1. Correlation of SEP peak intensities with various shock parameters. From left to right: peak intensities of <100 keVelectrons, ∼1 MeV electrons, and 60–100 MeV protons. From top to bottom: correlations with Alfvénic Mach number M_A, shock speed V_{sh}, and the shock speed at the leading edge of the CME V_{sh} (LE). The Pearson correlation coefficient cc is provided in each figure legend together with its uncertainty range corresponding to a 90% confidence interval (in square brackets) and the corresponding p-value (in round brackets).

2.3. The Relation of Electron Event Spectra with Shock Parameters

Dresing et al. (2020) focused on electron spectra in the near-relativistic range (45–425 keV), which often show broken-power-law shapes, and determined the spectral index at two reference energies (70 and 200 keV) for all events in their sample. No clear correlations were found between these spectral indices and the shock parameters (not shown), for example, a spectral hardening related with stronger shocks, which would explicitly point to shock acceleration. However, we suspect that this missing correlation is caused by a selection effect, as illustrated by Figure 3. It presents the histograms of the two reference spectral indices for the whole sample as in Dresing et al. (2020; blue) compared to the distribution of spectral indices of the 33 events analyzed in this study. The figure shows that the events analyzed here belong to those with the hardest energy spectra in the whole sample of electron events observed with STEREO during solar cycle 24. Almost all of the near-relativistic events are accompanied by relativistic electrons (see Table 1), proving the presence of efficient electron acceleration.

3. Discussion and Conclusions

Our analysis shows a clear correlation between the peak intensities of SEEs and key parameters of modeled shocks at the relevant cob-points. We analyzed the peak intensities of near-relativistic (55–85 keV) and relativistic (0.7–1.4 MeV) electrons and compared their correlations with several modeled shock parameters, such as Alfvénic and magnetosonic Mach numbers, shock speed (at the spacecraft magnetic footpoint and

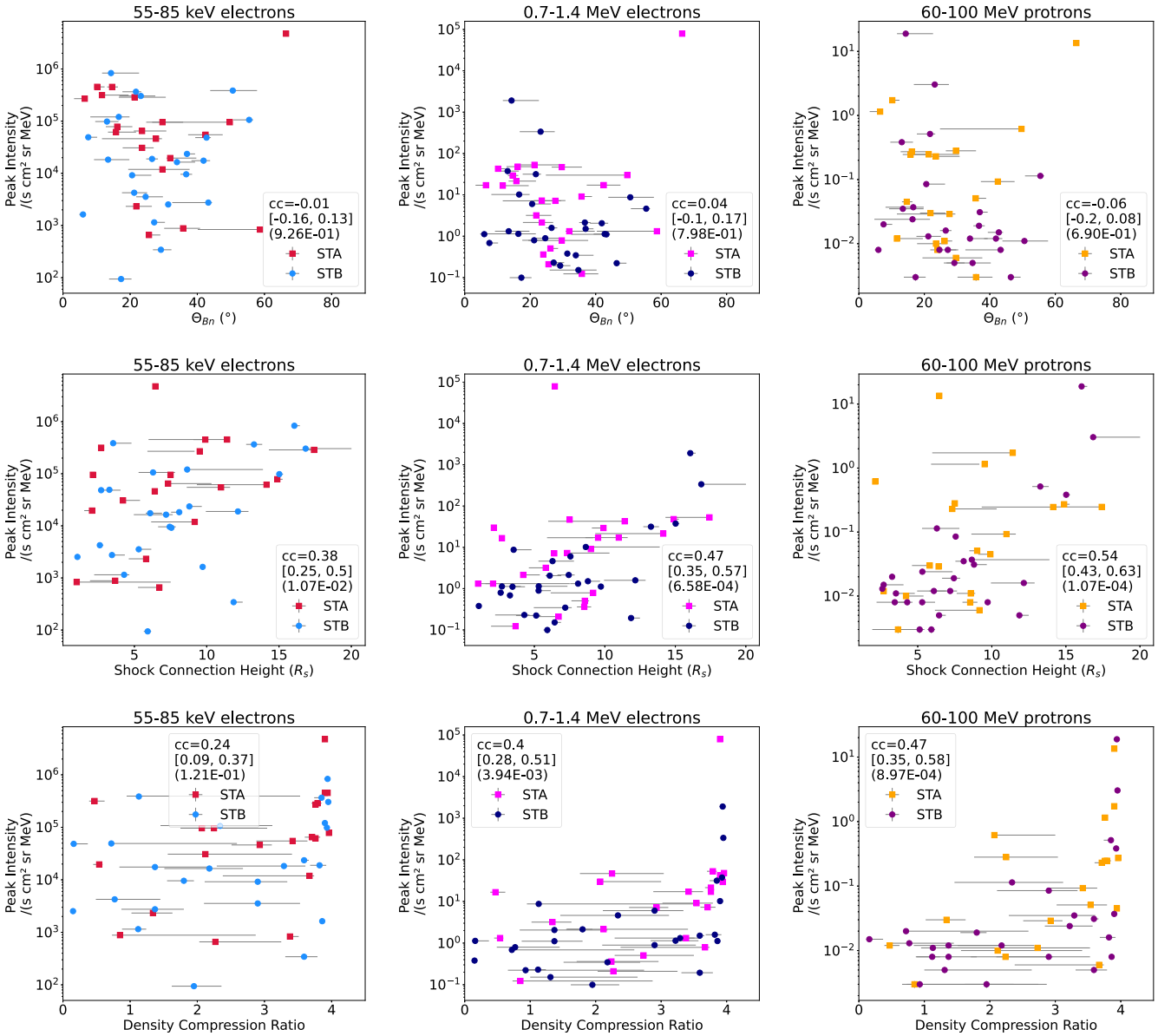

Figure 2. As in Figure 1 but for the magnetic field obliquity with respect to the shock normal Θ_{Bn} (top), the shock connection height above the photosphere (center), and the density compression ratio X (bottom).

the CME leading edge), magnetic field obliquity with respect to the shock normal (Θ_{Bn}), the height of shock at the time of maximum Mach number, and the density compression ratio.

As in Kouloumvakos et al. (2019) for protons, the strongest correlations occur with the Mach number; the Alfvénic Mach number yields the strongest correlations of cc = 0.69 for relativistic and cc = 0.47 for near-relativistic electrons, respectively. The correlations are weaker between near-relativistic electrons, with all other shock parameters as seen for 60–100 MeV protons. No correlation is found between peak intensities and shock obliquity, although there is a tendency for the highest electron peak intensities to occur during quasi-parallel to oblique shock.

Surprisingly, no difference between electrons and protons can be observed with respect to shock obliquity that would be expected from shock acceleration theory. Electrons should be preferentially accelerated by shock-drift acceleration at quasi-perpendicular shocks and protons by diffusive-shock acceleration at quasi-parallel shocks, respectively (e.g., Jokipii 1987; Burgess 2006). A rapidly changing shock geometry could induce important time-dependent effects of the acceleration process that are hard to assess without a detailed modeling effort, as indeed for most events the shock transits from an initially quasi-perpendicular to a quasi-parallel in the upper corona.

Our results show that the role of the shock for relativistic electrons is significant and of the same importance as for the high-energy protons, suggesting a common, shock-related acceleration process. This is also supported by the strong correlations between electron and proton peak intensities that are stronger for the relativistic than for the near-relativistic electrons

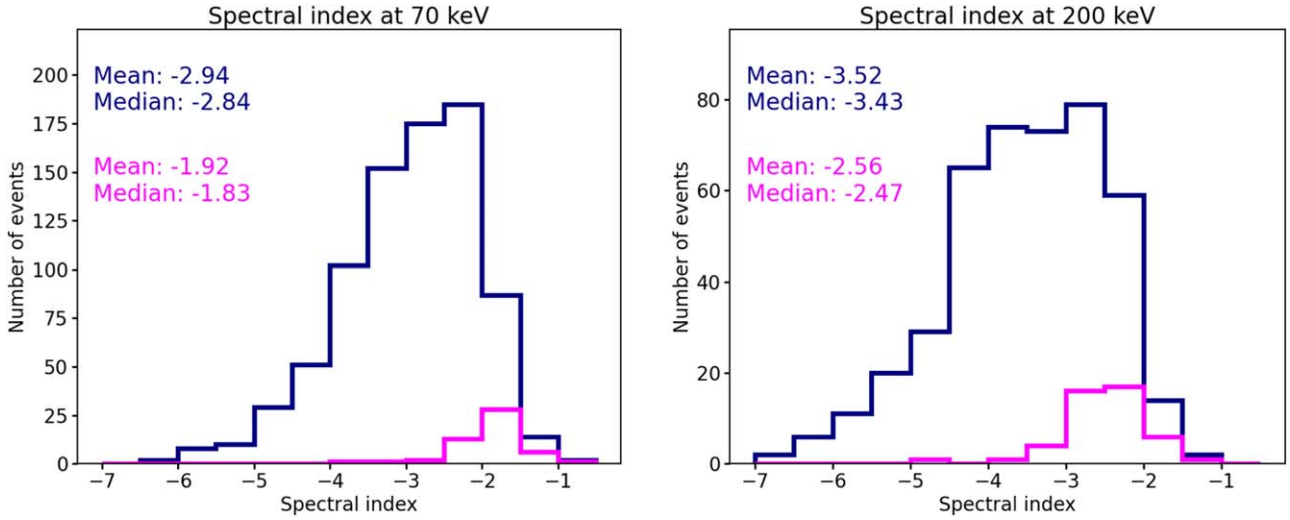

Figure 3. Histograms of spectral indices at reference energies of 70 keV (left) and 200 keV (right). Blue histograms correspond to the distribution of all STEREO/SEPT SEE events (Dresing et al. 2020), while magenta histograms represent the sample under study here.

Table 2
Pearson Correlation Coefficients between SEP Peak Intensities and Different Shock Parameters

CCs	SEPT e (55–85 keV)	HET e (0.7–1.4 MeV)	HET p (60–100 MeV)
(1)	(2)	(3)	(4)
M_A	0.47 (1.46E-03) [0.34, 0.57]	0.69, (2.29E-08) [0.62, 0.76]	0.72, (1.64E-08) [0.64, 0.78]
M_{fm}	0.43 (3.88E-03) [0.3, 0.54]	0.61, (2.48E-06) [0.52, 0.69]	0.65, (1.00E-06) [0.56, 0.73]
V_{sh}	0.33 (2.84E-02) [0.19, 0.46]	0.53, (7.08E-05) [0.43, 0.62]	0.57, (2.98E-05) [0.47, 0.66]
V_{sh} (LE)	0.24 (1.20E-01) [0.09, 0.37]	0.35, (1.36E-02) [0.22, 0.46]	0.28, (5.53E-02) [0.15, 0.41]
Θ_{Bn}	−0.01 (9.26E-01) [−0.16, 0.13]	0.04, (7.98E-01) [−0.1, 0.17]	−0.06, (6.90E-01) [−0.2, 0.08]
H_c	0.38 (1.07E-02) [0.25, 0.5]	0.47, (6.58E-04) [0.35, 0.57]	0.54, (1.07E-04) [0.43, 0.63]
X	0.24 (1.21E-01) [0.09, 0.37]	0.4, (3.94E-03) [0.28, 0.51]	0.47, (8.97E-04) [0.35, 0.58]
HET p (20 MeV)	0.86 (5.87E-14) [0.82, 0.9]	0.84, (4.22E-14) [0.79, 0.87]	⋯ ⋯
HET p (40 MeV)	0.82 (1.47E-11) [0.77, 0.86]	0.92, (2.55E-21) [0.9, 0.94]	⋯ ⋯
HET p (60 MeV)	0.76 (1.28E-08) [0.69, 0.82]	0.91, (5.17E-18) [0.88, 0.93]	⋯ ⋯

Note. *P*-values of the correlation coefficients are provided in parentheses, uncertainties of cc corresponding to a 90% confidence interval are shown below in square brackets. The three rows at the bottom show the correlation of proton peak intensities above 20, 40, and 60 MeV with those of the near-relativistic and relativistic electrons.

(Table 2). Because of the weaker correlations between the shock parameters and the near-relativistic electrons, we conclude that the role of the shock is smaller at these energies and another process must be involved in accelerating these lower-energy electrons, which is most likely flare-related (Dresing et al. 2021). The stronger correlation of near-relativistic electron intensities with the lower-energy proton intensities (e.g., HET-protons at 20 MeV; see Table 2) suggests that this other process could possibly contribute to those lower-energy proton fluxes as well. Figure 1 shows that the correlation of the near-relativistic electrons with the Alfvénic Mach Number seems to improve if only peak intensities above $\sim 10^4\,\mathrm{cm^{-2}\,sr^{-1}\,s^{-1}\,MeV^{-1}}$ are considered.

One might argue that the observed correlations with the shock parameters are only apparent because of the big flare syndrome (Kahler 1982), which postulates that, statistically, various solar activity phenomena are more intense during large flares. Therefore, a correlation with the CME or the CME-driven shock parameters might be found only because they correlate with the strength of the flare. We note, however, that this possibility is highly unlikely. The correlations found in this study are determined by the specific shock parameters at the cob-point. Correlating, for example, peak intensities observed at STEREO A with the Alfvénic Mach number determined at the magnetic footpoint of STEREO B yields completely vanishing correlations with $cc = 0.03$ and $cc = -0.13$ for $\sim$1 MeV and $<$100 keV electron peak intensities, respectively (not shown). Similarly, the shock parameters of STEREO A and STEREO B of the same events show only very weak correlations with each other (e.g., $cc = 0.17$ for the Alfvénic Mach number), and correlating the peak intensities with the global parameter of the shock speed at the CME leading edge (Figure 1, bottom row) yields smaller correlation coefficients than the correlations with the shock speeds at the respective magnetic footpoints (Figure 1, mid-row). In addition, we find a very weak correlation between the analyzed peak intensities and the strength of the flare. Correlation of the peak flare intensity measured in soft X-rays by the GOES spacecraft yields correlation coefficients of 0.26, 0.19, and 0.12 for 60–100 MeV protons, $\sim$1 MeV electrons, and $<$100 keV SEPT electrons (not shown). However, the statistical sample for these correlations is lower because the flare was only observed during 20 out of the 33 analyzed events.

No clear correlations were found between the shock parameters and the spectral indices of the near-relativistic (45–425 keV) electron events that are assumed to represent the efficiency of the underlying acceleration process. This missing correlation could be caused, on the one hand, by transport effects that modify the energy spectrum, e.g., particle scattering at magnetic field irregularities as described by Strauss et al. (2020). On the other hand, the analyzed event sample might suffer a

selection effect, which is demonstrated when comparing the spectral indices of the events studied here with the distribution of spectral indices of all SEE events observed with the STEREO spacecraft in solar cycle 24 (Dresing et al. 2020). This comparison (Figure 3) shows that the events studied here are among the most energetic events of the cycle, shown by the hardest electron spectra observed in the whole sample. This is also underlined by the presence of relativistic electrons for almost all events studied here. For comparison, only about 20% of all STEREO/SEPT electron events were accompanied by relativistic electrons (Dresing et al. 2020). New spacecraft measurements with higher energy resolution as provided, for example, by the Solar Orbiter Energetic Particle Detector suite (Rodríguez-Pacheco et al. 2020) might help to identify specific footprints of the shock in the electron energy spectra.

We conclude that the relativistic SEE events in the MeV range, studied here, are mainly produced by coronal shock acceleration, with the shock being as important as it is for solar energetic proton events in the >60 MeV range. However, we do not exclude the possibility that a flare-related process can also contribute to the acceleration with a smaller importance. For the SEEs at lower energies, we conclude that this population is probably a mixture of flare and shock-accelerated electrons with a larger contribution of the flare component compared to the higher-energy electrons.

This study was funded by the European Union's Horizon 2020 research and innovation program under grant agreement No. 101004159 (SERPENTINE). Work in the University of Turku was performed under the umbrella of Finnish Centre of Excellence in Research of Sustainable Space. N.D. is grateful for support by the Turku Collegium for Science, Medicine and Technology of the University of Turku, Finland. A.K. acknowledges financial support from the SERPENTINE project and the ANR COROSHOCK project (ANR-17-CE31-0006-01). We also acknowledge support from the French space agency Centre National des Etudes Spatiales (CNES, https://cnes.fr/fr) that supports the Solar-Terrestrial Observations and Modeling Service (STORMS, http://storms-service.irap.omp.eu/) exploited for the modeling part of this study. We also thank Predictive Sciences Inc. for making their 3D MHD model continuously available through their website.

ORCID iDs

Nina Dresing https://orcid.org/0000-0003-3903-4649
Athanasios Kouloumvakos https://orcid.org/0000-0001-6589-4509
Rami Vainio https://orcid.org/0000-0002-3298-2067
Alexis Rouillard https://orcid.org/0000-0003-4039-5767

References

Burgess, D. 2006, ApJ, 653, 316
Cane, H. V., McGuire, R. E., & von Rosenvinge, T. T. 1986, ApJ, 301, 448
Dresing, N., Effenberger, F., Gómez-Herrero, R., et al. 2020, ApJ, 889, 143
Dresing, N., Gómez-Herrero, R., Heber, B., et al. 2018, A&A, 613, A21
Dresing, N., Theesen, S., Klassen, A., & Heber, B. 2016, A&A, 588, A17
Dresing, N., Warmuth, A., Effenberger, F., et al. 2021, A&A, 654, A92
Gopalswamy, N., Yashiro, S., Krucker, S., Stenborg, G., & Howard, R. A. 2004, JGRA, 109, A12105
Haggerty, D. K., & Roelof, E. C. 2002, ApJ, 579, 841
Haggerty, D. K., & Roelof, E. C. 2009, in AIP Conf. Ser. 1183, SHOCK WAVES IN SPACE AND ASTROPHYSICAL ENVIRONMENTS: 18th Annual International Astrophysics Conference, Probing SEP Acceleration Processes With Near-relativistic Electrons, ed. X. Ao & G. Z. R. Burrows (New York: AIP), 3
Jokipii, J. R. 1987, ApJ, 313, 842
Kahler, S. W. 1982, JGR, 87, 3439
Kahler, S. W. 2007, SSRv, 129, 359
Kahler, S. W., Aurass, H., Mann, G., & Klassen, A. 2007, ApJ, 656, 567
Klein, K. L., Krucker, S., Trottet, G., & Hoang, S. 2005, A&A, 431, 1047
Kouloumvakos, A., Nindos, A., Valtonen, E., et al. 2015, A&A, 580, A80
Kouloumvakos, A., Rouillard, A. P., Wu, Y., et al. 2019, ApJ, 876, 80
Krucker, S., Kontar, E. P., Christe, S., & Lin, R. P. 2007, ApJL, 663, L109
Lionello, R., Linker, J. A., & Mikić, Z. 2009, ApJ, 690, 902
Mann, G. 2015, JPlPh, 81, 475810601
Mann, G., Melnik, V. N., Rucker, H. O., Konovalenko, A. A., & Brazhenko, A. I. 2018, A&A, 609, A41
Masters, A., Stawarz, L., Fujimoto, M., et al. 2013, NatPh, 9, 164
Müller-Mellin, R., Böttcher, S., Falenski, J., et al. 2007, SSSRv, 136, 371
Papaioannou, A., Sandberg, I., Anastasiadis, A., et al. 2016, JSWSC, 6, A42
Posner, A. 2007, SpWea, 5, 05001
Reames, D. V. 1999, SSRv, 90, 413
Reames, D. V. 2021a, Solar Energetic Particles. A Modern Primer on Understanding Sources, Acceleration and Propagation, 978 (Cham: Springer)
Reames, D. V. 2021b, FrASS, 8, 164
Riley, P., Lionello, R., Linker, J. A., et al. 2011, SoPh, 274, 361
Rodríguez-Pacheco, J., Wimmer-Schweingruber, R. F., Mason, G. M., et al. 2020, A&A, 642, A7
Rouillard, A. P., Plotnikov, I., Pinto, R. F., et al. 2016, ApJ, 833, 45
Rouillard, A. P., Sheeley, N. R., Tylka, A., et al. 2012, ApJ, 752, 44
Sarris, E. T., & Krimigis, S. M. 1985, ApJ, 298, 676
Simnett, G. M. 2003, SoPh, 213, 387
Strauss, R. D., Dresing, N., Kollhoff, A., & Brüdern, M. 2020, ApJ, 897, 24
Trottet, G., Samwel, S., Klein, K. L., Dudok de Wit, T., & Miteva, R. 2015, SoPh, 290, 819
Tsurutani, B. T., & Lin, R. P. 1985, JGR, 90, 1
von Rosenvinge, T. T., Reames, D. V., Baker, R., et al. 2008, SSRv, 136, 391
Wang, W., Wang, L., Krucker, S., et al. 2021, ApJ, 913, 89
Yang, L., Wang, L., Li, G., et al. 2019, ApJ, 875, 104